ROYAL SOCIETY OPEN SCIENCE

rsos.royalsocietypublishing.org

Research

Cite this article: Wang C, Hu L, Wang M, Yue B, He H. 2018 Cerium promoted V-g-C_3N_4 as highly efficient heterogeneous catalysts for the direct benzene hydroxylation. *R. Soc. open sci.* **5**: 180371.
http://dx.doi.org/10.1098/rsos.180371

Received: 7 March 2018
Accepted: 16 May 2018

Subject Category:
Chemistry

Subject Areas:
green chemistry/materials science

Keywords:
carbon nitride, cerium, vanadium, benzene hydroxylation

Authors for correspondence:
Bin Yue
e-mail: yuebin@fudan.edu.cn
Heyong He
e-mail: heyonghe@fudan.edu.cn

This article has been edited by the Royal Society of Chemistry, including the commissioning, peer review process and editorial aspects up to the point of acceptance.

Electronic supplementary material is available online at https://dx.doi.org/10.6084/m9.figshare.c.4123382.

THE ROYAL SOCIETY PUBLISHING

Cerium promoted V-g-C_3N_4 as highly efficient heterogeneous catalysts for the direct benzene hydroxylation

Cheng Wang, Liya Hu, Meiyin Wang, Bin Yue and Heyong He

Department of Chemistry and Shanghai Key Laboratory of Molecular Catalysis and Innovative Materials, Collaborative Innovation Center of Chemistry for Energy Materials, Fudan University, Shanghai 200433, China

HH, 0000-0002-1781-6255

A series of Ce_x-V-g-C_3N_4 catalysts with different cerium content were synthesized by a facile co-assembly method. Compared with pure V-g-C_3N_4 catalyst, the addition of cerium facilitated the high dispersion of vanadium species as well as the benzene adsorption ability of the corresponding catalysts. Also, the existence of cerium promoted the partial reduction of vanadium species, which improved the redox property of vanadium species as the active centres. The Ce_x-V-g-C_3N_4 catalysts showed considerably improved activity in the benzene hydroxylation reaction compared with V-g-C_3N_4 catalyst. Among the catalysts studied, $Ce_{0.07}$-0.07 V-g-C_3N_4 exhibited the best catalytic activity with a benzene conversion of 33.7% and a phenol yield of 32.3% with good structural and catalytic stability, while only 24.7% of benzene conversion and phenol yield of 24.2% were obtained over 0.07 V-g-C_3N_4.

1. Introduction

Phenol, as an important chemical intermediate in industry, is widely employed in the synthesis of aniline, resins, plastics, bactericides and agrochemicals [1]. However, the current phenol production is based upon the three-step cumene process, which has some inevitable disadvantages, e.g. the by-product acetone with low market demand, the complex synthesis steps and the high energy consumption [2]. From the view of green chemistry, the direct hydroxylation of benzene to phenol has attracted great interest in the past few decades.

Since it is difficult to insert an oxygen atom into the stable C−H bond of benzene, many efforts have been devoted to searching for appropriate oxidants [3]. Among them, molecular oxygen, nitrous oxide and hydrogen peroxide are three main kinds of oxidants used in the benzene hydroxylation reaction [4–7]. However, molecular oxygen is too stable to be activated mildly, while nitrous oxide is not easily available in industry. In contrast, hydrogen peroxide shows superior properties with the mild reaction condition of benzene oxidation and water as the green by-product.

Up to now, catalysts with various metal species, such as V, Fe, Cu, Co and Ti [8–12], have been employed for this titled reaction. Among them, vanadium species exhibit excellent catalytic activity. As for the catalyst support, many metal oxides such as Al_2O_3, SiO_2 and TiO_2 were widely used [13–15]. However, the weak interaction between V species and the metal oxide support leads to undesirable loss of V active spices [16]. Besides, some metal oxide supports, such as Al_2O_3 and ZrO_2, disfavour the redox cycle between V^{5+} and V^{4+} [17,18], leading to the low activity in the direct oxidation of benzene to phenol.

Nowadays, graphitic carbon nitride (g-C_3N_4), as an analogue of graphene, has been widely used as a catalyst support, due to its unique physico-chemical property and easily modified feature. Compared with pure graphene, the N-containing groups with strong coordination ability may facilitate the dispersion and stability of metal species. Moreover, carbon support will show certain reduction ability at high temperature, affecting the valence state of loaded metal species [19–21]. In previous work [22], we found that V^{5+} species were partially reduced to V^{4+} ones during the calcination process over g-C_3N_4 support. And the resulting V-g-C_3N_4 catalyst showed excellent catalytic performance and stability in the direct benzene hydroxylation. As is known, the transformation between V^{5+} and V^{4+} species plays an important role in the benzene conversion. Therefore, it is worth exploring the proper molar ratio of V^{4+}/V^{5+} to obtain the most effective catalyst for the titled reaction.

Recently, bi-metal or multi-metal catalysts have shown competitive advantages in redox reactions. As the most abundant rare earth element, cerium is widely used in catalytic oxidation due to its unique electronic structures. The different electronic configurations between Ce^{3+} with $4f^15d^0$ and Ce^{4+} with $4f^05d^0$ lead to the formation of good redox couple of Ce^{3+}/Ce^{4+} [23]. Paz *et al.* found that the addition of second metal cerium enhanced the interactions between Pt^0 and oxygen atoms. As a result, the bi-metal catalyst showed higher activity in the CO oxidation reaction even at lower reaction temperature compared with the non-promoted Pt catalysts [24]. Lu *et al.* prepared a series of CeO_2–Co_3O_4 catalysts for the catalytic oxidation of formaldehyde (HCHO) [25]. The unique redox property of Ce played a crucial role in the excellent performance in HCHO oxidation.

In this study, we added cerium as the second metal into V supported g-C_3N_4 in order to facilitate the redox property of V species. A series of cerium-doped V-g-C_3N_4 catalysts were prepared by a facile co-assembly method using vanadylacetylacetonate, cerium nitrate and melamine as precursors. All the Ce doped V-g-C_3N_4 catalysts showed higher activity than the mono-metal ones. The strong synergistic effects between Ce and V result in the excellent redox property of V species, which improves the catalytic performance of corresponding catalysts in benzene hydroxylation.

2. Material and methods

2.1. Synthesis

Melamine, vanadylacetylacetonate ($C_{10}H_{14}O_5V$) and $Ce(NO_3)_3{\cdot}6H_2O$ were all purchased from Aladdin Industrial Corporation and used without further purification. g-C_3N_4 was prepared by the direct calcination of melamine at 550°C for 2 h under nitrogen atmosphere [26]. 0.07 V-g-C_3N_4 sample was obtained as follows: 0.42 g of $C_{10}H_{14}O_5V$ and 2.50 g of melamine were mixed with 50 ml of ethanol. After stirring vigorously at 50°C for 1 h, the solution was dried at 60°C overnight. The resulting solid sample was calcined in N_2 from room temperature to 550°C with a heating rate of 2°C min^{-1} and kept at 550°C for another 2 h. After cooling to room temperature, the product was collected and denoted as 0.07 V-g-C_3N_4, where 0.07 represented the theoretical weight content of vanadium. 0.05 V-g-C_3N_4 and 0.10 V-g-C_3N_4 catalysts were prepared according to the same synthesis procedure as for 0.07 V-g-C_3N_4 by adding desired amount of $C_{10}H_{14}O_5V$.

As for 0.07Ce-g-C_3N_4, the synthesis method was also similar to that of 0.07 V-g-C_3N_4, except for adding 0.23 g of $Ce(NO_3)_3{\cdot}6H_2O$ rather than 0.42 g of $C_{10}H_{14}O_5V$. Furthermore, by adding both 0.42 g of $C_{10}H_{14}O_5V$ and different amounts of $Ce(NO_3)_3{\cdot}6H_2O$, Ce_x-0.07 V-g-C_3N_4 catalysts were obtained, where x represents the molar ratio of Ce/V.

2.2. Benzene hydroxylation reaction

The direct benzene hydroxylation reaction was conducted as follows. Typically, 1 ml of benzene, 10 ml of 80 wt% acetic acid and 40 mg of catalyst were added into a 25 ml three-necked flask connected with a reflux condenser. After heating to 70°C, 3.5 ml of 30 wt% H_2O_2 was added dropwise in 30 min with vigorously stirring. The reaction mixture was stirred for another 4 h. After reaction, the catalyst was separated by centrifugation and the content of liquid products was analysed immediately by gas chromatography using toluene as the internal standard.

2.3. Material characterization

Elemental analysis was performed with a Thermo Elemental IRIS Intrepid inductively coupled plasma-atomic emission spectrometer (ICP-AES). Transmission electron microscopic (TEM) images were acquired with a FEI Tecnai G^2 F20 S-Twin field-emission transmission electron microscope operated at 200 kV. Elemental mapping was conducted using a Philips XL 30 microscope with energy dispersive X-ray spectrometer operated at 30 kV. Fourier transform infrared (FT-IR) spectra were recorded with a Nicolet iS10 infrared instrument using KBr discs. X-ray diffraction (XRD) patterns were recorded on a Bruker D8 Advances X-ray diffractometer using Cu-Kα radiation with a voltage of 40 kV and a current of 40 mA. X-ray photoelectron spectra (XPS) were recorded with a Perkin-Elmer PHI 5000C ESCA system equipped with a dual X-ray source by using Mg Kα (1253.6 eV) anode and a hemispherical energy analyser. Specific surface area results were obtained at 77 K using a Micromeritics Tristar 3000 apparatus. The benzene adsorption was measured using a Hiden intelligent gravimetric analyser. All samples were degassed under a vacuum of less than 10^{-3} Pa at 300°C for 6 h prior to the adsorption measurement.

3. Results and discussion

The results of benzene hydroxylation reaction over all catalysts studied are shown in table 1 and electronic supplementary material, table S1. By optimizing the vanadium content in the catalysts, the best catalytic activity in the benzene hydroxylation reaction was obtained over 0.07 V-g-C_3N_4 catalyst with 7 wt% of vanadium content. With the introduction of cerium into the 0.07 V-g-C_3N_4 catalyst (Ce/V = 0.05), the benzene conversion is improved slightly from 24.7% to 25.3% (entry 2, table 1). With the further rise of cerium content, the benzene conversion increases remarkably to the highest 33.7% over $Ce_{0.07}$-0.07 V-g-C_3N_4 (entry 3, table 1) and then decreases to 29.4% over $Ce_{0.10}$-0.07 V-g-C_3N_4 (entry 4, table 1), while the phenol selectivity remains almost constant with the variation of cerium content. Moreover, the carbon balance value shown in table 1 are greater than 99% over the three Ce-containing catalysts, indicating a high carbon yield with negligible side reactions. The TOF value of 17.1 h^{-1} based on the vanadium content also indicates that $Ce_{0.07}$-0.07 V-g-C_3N_4 is the most active catalyst. Thus, we deduce that a proper molar ratio of Ce/V possibly facilitates both the redox properties of V species and the efficient decomposition of H_2O_2, leading to the remarkable catalytic activity in the benzene conversion reaction [27].

In order to elucidate the synergistic effects between V and Ce species, we selected g-C_3N_4, 0.07 V-g-C_3N_4 and $Ce_{0.07}$-0.07 V-g-C_3N_4 as the representative catalysts to carry out detailed characterizations. Generally, the specific surface area of a catalyst has a certain influence on the catalytic activity. As shown in table 2, the specific surface area increases slightly after the introduction of metal species compared with that of the non-modified g-C_3N_4 catalyst (entries 1–3) and $Ce_{0.07}$-0.07 V-g-C_3N_4 has the highest specific surface area. However, the quite different catalytic performances between 0.07 V-g-C_3N_4 and $Ce_{0.07}$-0.07 V-g-C_3N_4 demonstrate that the specific surface area is not the main reason for the different catalytic activity.

The morphologies of the catalysts were studied by TEM. As shown in figure 1*a–d*, all the samples exhibit the typical large lamellar structure, indicating that the structure of g-C_3N_4 support remains after the incorporation of metal species. As for 0.07 V-g-C_3N_4 and $Ce_{0.07}$-0.07 V-g-C_3N_4 catalysts (figure 1*b–d*), no obvious metal particles are observed over both catalysts, implying the high dispersion of metal species. Also, the element-mapping images of 0.07 V-g-C_3N_4 and $Ce_{0.07}$-0.07 V-g-C_3N_4 catalysts (figure 1*e–g*) further demonstrate that both V and Ce species are highly dispersed over the g-C_3N_4 support.

However, it is worth noting that the vanadium dispersion of 0.07 V-g-C_3N_4 is slightly poorer than that of $Ce_{0.07}$-0.07 V-g-C_3N_4. This implies that the existence of cerium may facilitate the high dispersion of vanadium, leading to the high catalytic activity [28].

Table 1. Catalytic activity of various catalysts for benzene hydroxylation reaction. Reaction conditions: 1 ml of benzene, 10 ml of 80 wt% acetic acid, 40 mg of catalyst, 3.5 ml of 30 wt% H_2O_2, 70°C for 4 h.

							carbon out (mmol)			
entry	catalyst	benzene conv. (%)	phenol select. (%)	phenol yield (%)	TOF[a] value (h^{-1})	carbon in (mmol)	unreacted benzene	phenol	by-products[b]	carbon balance closure[c] (%)
1	0.07 V-g-C_3N_4	24.7	98.1	24.2	12.4	67.6	50.9	16.4	0.2	>99
2	$Ce_{0.05}$-0.07 V-g-C_3N_4	25.3	96.3	24.4	12.7	67.6	50.5	16.5	0.5	>99
3	$Ce_{0.07}$-0.07 V-g-C_3N_4	33.7	95.9	32.3	17.1	67.6	44.8	21.8	0.9	>99
4	$Ce_{0.10}$-0.07 V-g-C_3N_4	29.4	97.6	28.7	15.1	67.6	47.7	19.4	0.5	>99

[a]Turnover frequency (TOF) was calculated as the molecules of generated phenol per metal atom per hour.
[b]The total amount of hydroquinone and catechol.
[c]The carbon balance closure was calculated as the molar ratio of carbon out to carbon in.

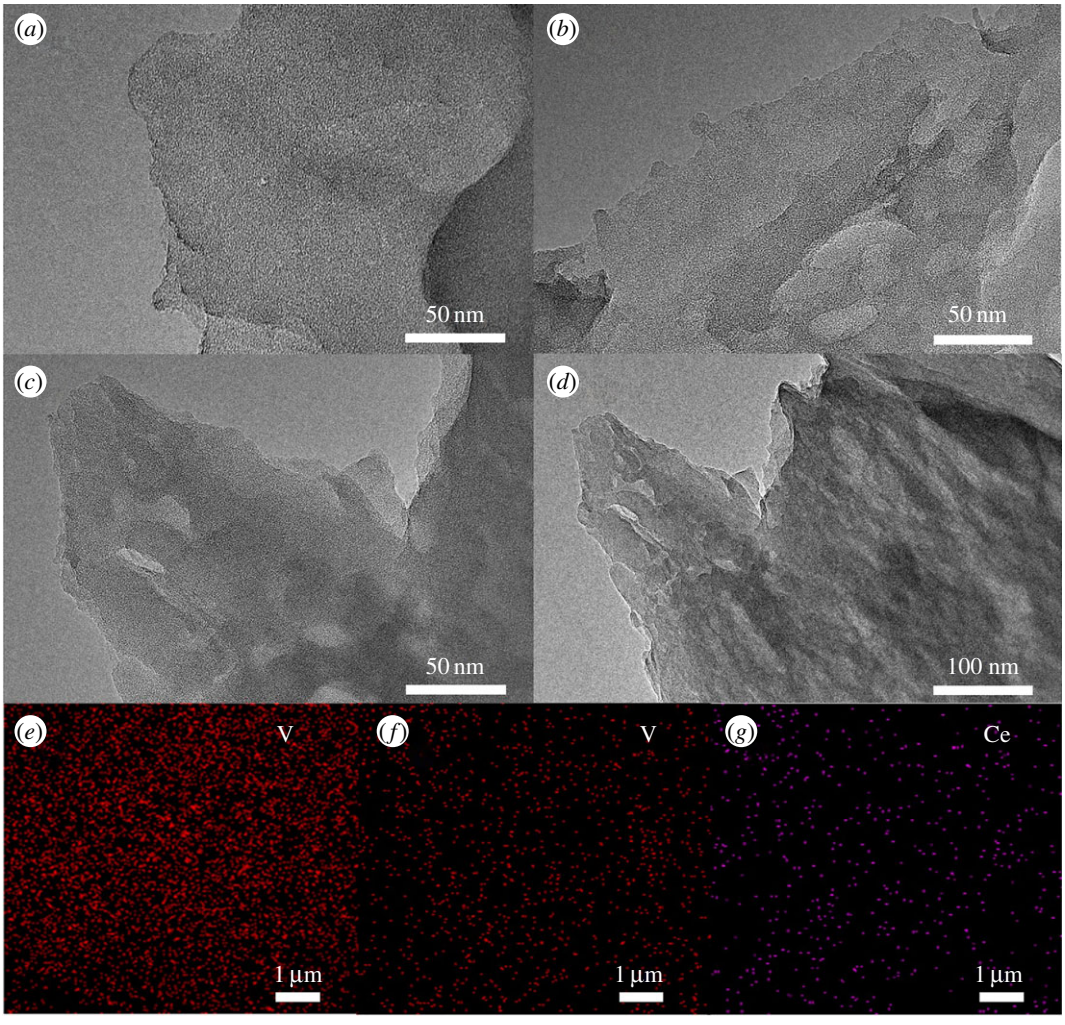

Figure 1. TEM images of (*a*) g-C_3N_4. (*b*) 0.07 V-g-C_3N_4 and (*c*,*d*) $Ce_{0.07}$-0.07 V-g-C_3N_4. V mapping of (*e*) 0.07 V-g-C_3N_4 and (*f*) $Ce_{0.07}$-0.07 V-g-C_3N_4 and Ce mapping of (*g*) $Ce_{0.07}$-0.07 V-g-C_3N_4.

Table 2. Specific surface area and metal contents of various catalysts.

entry	catalyst	S_{BET} ($m^2\ g^{-1}$)	vanadium content (wt.%)[a]	cerium content (wt.%)[a]
1	g-C_3N_4	32	—	—
2	0.07 V-g-C_3N_4	43	7.0	—
3	$Ce_{0.07}$-0.07 V-g-C_3N_4	47	6.8	0.5

[a]Analysed by ICP-AES.

The graphitic stacking structures of the catalysts were also confirmed by XRD patterns. For pure g-C_3N_4 (electronic supplementary material, figure S1*a*), two distinct diffractions are observed at *ca* 13.2° and 27.5°, corresponding to (100) diffraction of in-planar repeating motifs of tris-*s*-triazine units and (002) diffraction of interlayer stacking aromatic systems, respectively [29]. After the addition of metal species, both corresponding (100) and (002) diffraction peaks become broader, suggesting that the ordered structure of g-C_3N_4 support decreases slightly. In addition, the (002) peaks of 0.07 V-g-C_3N_4 and $Ce_{0.07}$-0.07 V-g-C_3N_4 catalysts both shift to low angle slightly compared with that of g-C_3N_4, indicating that the metal oxides were incorporated into the g-C_3N_4 sheets successfully [30]. Furthermore, no distinct peak originating from either vanadium or cerium species can be observed, which implies that the metal species are in non-crystallized state or dispersed well on the g-C_3N_4 layers. These results are consistent with the results of TEM.

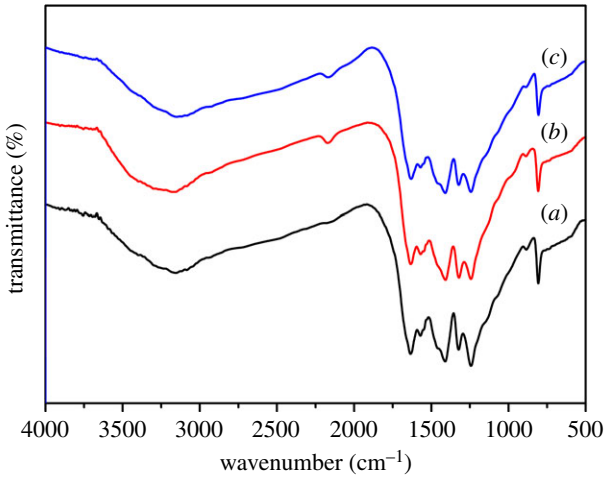

Figure 2. FT-IR spectra of (*a*) g-C_3N_4, (*b*) 0.07 V-g-C_3N_4 and (*c*) $Ce_{0.07}$-0.07 V-g-C_3N_4.

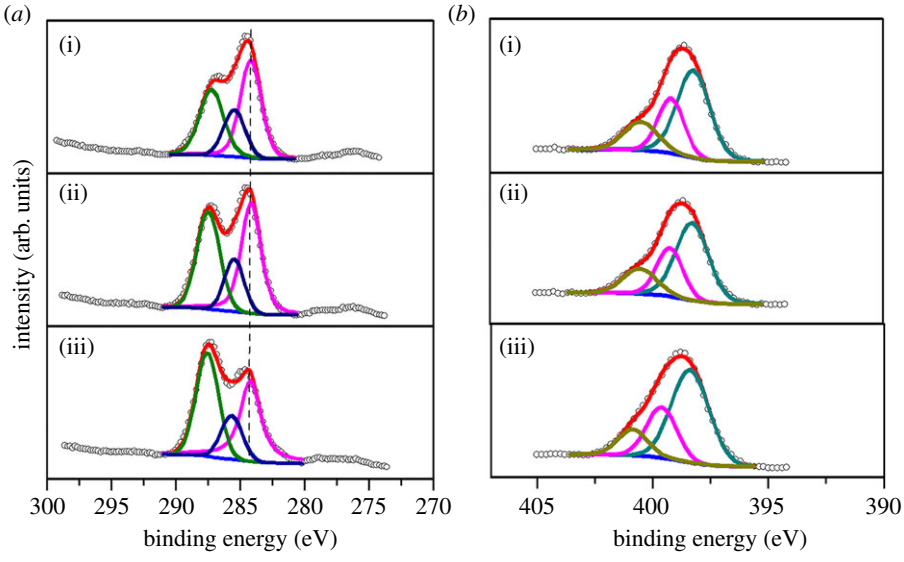

Figure 3. High resolution XPS spectra of C 1s (*a*) and N 1s (*b*) of (i) g-C_3N_4, (ii) 0.07 V-g-C_3N_4 and (iii) $Ce_{0.07}$-0.07 V-g-C_3N_4.

The FT-IR spectra of g-C_3N_4, 0.07 V-g-C_3N_4 and $Ce_{0.07}$-0.07 V-g-C_3N_4 catalysts are shown in figure 2. As for g-C_3N_4 (figure 2*a*), the major bands between 1200 and 1650 cm^{-1} are attributed to the stretching modes of CN heterocycles, while the band at 804 cm^{-1} corresponds to the stretching mode of triazine units (C_6N_7). The broad bands in the range of 3000–3400 cm^{-1} can be ascribed to the stretching of N−H bonds in both uncondensed amino groups and adsorbed water molecules [31]. For 0.07 V-g-C_3N_4 and $Ce_{0.07}$-0.07 V-g-C_3N_4 (figure 2*b*,*c*), their spectra are similar to that of g-C_3N_4 except for a small additional band at 2157 cm^{-1} corresponding to the disturbance of conjugated N=C−N units after metal doping [32,33].

In order to investigate the surface chemical composition of the catalysts, XPS measurement was carried out. As shown in electronic supplementary material, figure S2, C and N species, which refer to the peaks at binding energies of 288.0 (C 1s) and 400.0 (N 1s), are the main elements in all catalysts. By subtracting the peak area of the contaminant carbon C 1s at 284.6 eV, the peak area ratios of C 1s/N 1s of g-C_3N_4, 0.07 V-g-C_3N_4 and $Ce_{0.07}$-0.07 V-g-C_3N_4 catalysts are 0.89, 0.83 and 0.73, respectively. As the theoretical molar ratio of C/N in g-C_3N_4 is 3/4, the correction factor between peak area ratio of C/N and molar ratio of C/N should be 1.187. Based on the correction factor, the C/N molar ratio of 0.07 V-g-C_3N_4 and $Ce_{0.07}$-0.07 V-g-C_3N_4 can be calculated as 3/4.3 and 3/4.9, respectively, which implies the formation of N-rich carbon nitride by the incorporation of metal species. The reason for

Table 3. The ratios of V species with different valence states on the catalyst surface.

entry	catalyst	V^{4+}/V^{5+}	$(V^{4+}+V^{3+})/V^{5}$	V^{3+}/V^{4+}
1	0.07 V-g-C_3N_4	0.45	0.45	—
2	$Ce_{0.05}$-0.07 V-g-C_3N_4	0.53	0.93	0.78
3	$Ce_{0.07}$-0.07 V-g-C_3N_4	0.62	1.09	0.75
4	$Ce_{0.10}$-0.07 V-g-C_3N_4	0.64	1.15	0.74
5	0.07 V-g-C_3N_4 recycled	0.48	0.48	—
6	$Ce_{0.07}$-0.07 V-g-C_3N_4 recycled	0.49	0.85	0.73

the C/N molar ratio variation may be caused by the increase of –NH groups on the g-C_3N_4 support surface as the metal species destroy the ordered structure of g-C_3N_4 partially. As reported previously, in preparation of C−N materials, the addition of metal species restrained the decomposition of nitrogen species and accelerated the decomposition of carbon species, leading to high N content in the samples [34,35]. As shown in figure 3*a*, the C 1s spectrum of g-C_3N_4 can be deconvoluted into three peaks with binding energies of 284.6, 285.7 and 287.5 eV, corresponding to the graphitic carbon (C−C), C−O and sp^2 hybridized carbon (N−C=N), respectively [36]. After the incorporation of metal species, the peak intensities of both C−O and N−C=N increase, while that of C−C decreases. These imply that the rigid structural regularity of g-C_3N_4 was partially broken and more defects were produced on the surface of g-C_3N_4, generating more sites for metal species anchoring. In figure 3*b*, the N 1s spectrum of g-C_3N_4 shows three main peaks at 398.2, 399.3 and 400.6 eV, assigned to triazine nitrogen (C=N−C), tertiary nitrogen (N−$(C)_3$) and amino function group (N−H), respectively [37]. It is worth noting that both the C 1s and N 1s peak positions of 0.07 V-g-C_3N_4 and $Ce_{0.07}$-0.07 V-g-C_3N_4 are slightly shifted to high binding energy regions compared with those of g-C_3N_4. Since the graphite analogue CN matrix is believed to stabilize the metal species with the 'coordination nest' consisting of C and N atoms [38], it is reasonable to deduce that a strong interaction between metal species and g-C_3N_4 support may exist, which is reflected in the XPS study. In addition, as shown in the V $2p_{3/2}$ XPS spectra (figure 4), 0.07 V-g-C_3N_4 merely contains V^{5+} and V^{4+}, while V^{3+} species appears in $Ce_{0.07}$-0.07 V-g-C_3N_4. Also, the content of low oxidation state V (V^{4+}, V^{3+}) species increases after the addition of cerium (figure 4*b–d*). These may be ascribed to the reduction of partial V^{5+} species by the Ce^{3+} species during calcination [39]. In fact, similar results were reported for other Ce–V catalysts [40,41]. As listed in table 3, the $(V^{4+}+V^{3+})/V^{5+}$ ratio (calculated by the corresponding area ratio) increases gradually from 0.45 to 1.15 with the increase of cerium content, corresponding to the rise of low oxidation state vanadium species. It seems that Ce^{3+}/Ce^{4+} species play an important role in maintaining the content of V^{4+} and V^{3+} species. During the oxidation of benzene to phenol over vanadium-containing catalyst using H_2O_2 as an oxidant, the low valent vanadium species can be oxidized to V^{5+}-O-O• or V^{4+}-O-O• radicals which perform as main active centres for the conversion of benzene to phenol [42]. In electronic supplementary material, figure S5, the V $2p_{3/2}$ XPS measurements of both 0.07 V-g-C_3N_4 and $Ce_{0.07}$-0.07 V-g-C_3N_4 catalysts were conducted after four recycles. The recovered $Ce_{0.07}$-0.07 V-g-C_3N_4 catalyst shows little change in the ratios of $(V^{4+}+V^{3+})/V^{5+}$ and V^{3+}/V^{4+} relative to the fresh one, indicating that the excellent redox ability of Ce^{3+}/Ce^{4+} improves the redox cycles of V^{5+}/V^{4+} and V^{4+}/V^{3+}. Comparing with $Ce_{0.07}$-0.07 V-g-C_3N_4, the recovered $Ce_{0.07}$-0.07 V-g-C_3N_4 catalyst has small amount of Ce^{4+} species with the appearance of Ce^{4+} fingerprint (electronic supplementary material, figure S6) [43]. The existence of Ce^{3+}/Ce^{4+} is confirmed, which promotes the formation of low state vanadium. However, •OH radicals produced by V^{4+} lead to overoxidation of benzene [44]. It is believed that V^{4+} species are more reactive than V^{5+} ones during the benzene conversion [45]. Thus a proper molar ratio of $(V^{4+}+V^{3+})/V^{5+}$ may be beneficial to achieve a good conversion of benzene and a high selectivity of phenol. Therefore, in the present case, it is reasonable to indicate that the addition of proper cerium amount improves the redox capacity of active vanadium species along with the efficient decomposition of hydrogen peroxide.

The adsorption properties of g-C_3N_4, 0.07 V-g-C_3N_4 and $Ce_{0.07}$-0.07 V-g-C_3N_4 catalysts were evaluated by studying the gravimetric uptake of benzene. In figure 5*a*, pure g-C_3N_4 exhibits an evident adsorption of benzene, probably attributed to the strong π–π interactions between benzene molecules and g-C_3N_4 [28]. Interestingly, $Ce_{0.07}$-0.07 V-g-C_3N_4 exhibits the highest benzene adsorption ability among all the catalysts. As reported earlier [46,47], by increasing the content of surface basic groups

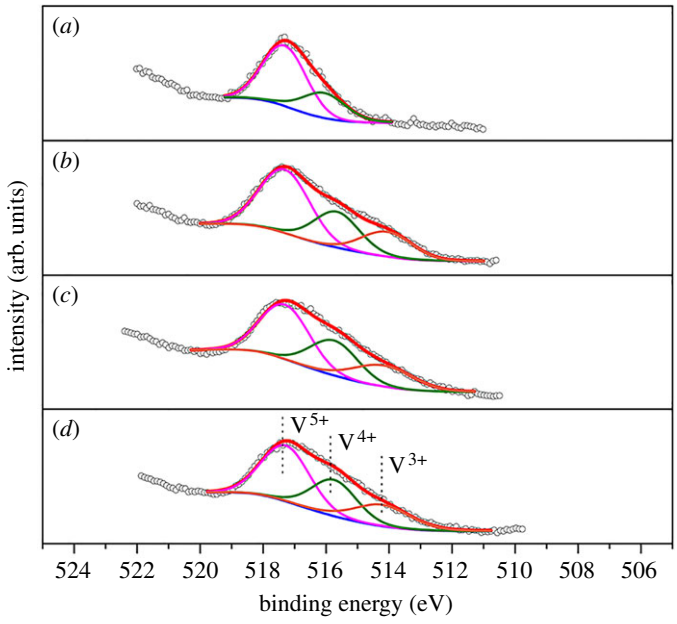

Figure 4. V $2p_{3/2}$ XPS spectra of (*a*) 0.07 V-g-C_3N_4, (*b*) $Ce_{0.05}$-0.07 V-g-C_3N_4, (*c*) $Ce_{0.07}$-0.07 V-g-C_3N_4 and (*d*) $Ce_{0.10}$-0.07 V-g-C_3N_4.

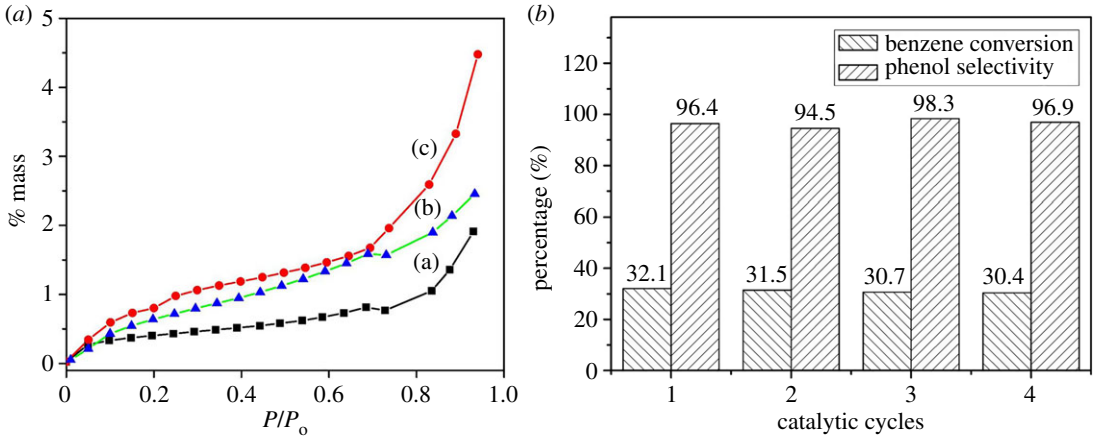

Figure 5. (*a*) The benzene adsorption isotherms of (a) g-C_3N_4, (b) 0.07 V-g-C_3N_4, (c) $Ce_{0.07}$-0.07 V-g-C_3N_4 at 298 K. (*b*) Cyclic utilization of $Ce_{0.07}$-0.07 V-g-C_3N_4.

(e.g. amino or hydroxyl groups) in activated carbon, the adsorption affinity for the nonpolar molecules, e.g. benzene, was enhanced. Therefore, combining with the results of XPS, it is reasonable to deduce that the increase of nitrogen-containing groups in g-C_3N_4 support after doping metal species can promote the benzene adsorption ability of the corresponding catalyst effectively, leading to the excellent benzene conversion.

The reusability of $Ce_{0.07}$-0.07 V-g-C_3N_4 catalyst was investigated as it showed the best catalytic activity in the target reaction (figure 5*b*). After each reaction, the $Ce_{0.07}$-0.07 V-g- C_3N_4 catalyst was separated, washed and dried for the next fresh reaction. After four recycles, the catalyst retained high activity without marked loss in both benzene conversion and phenol selectivity. The vanadium content of both the last recycled catalyst and the reaction solution was measured by ICP-AES, and no leaching of vanadium happened (entry 9, electronic supplementary material, table S1). In table 3, as expected, the $(V^{4+} + V^{3+})/V^{5+}$ peak area ratio of recovered $Ce_{0.07}$-0.07 V-g-C_3N_4 is 0.85, much higher than that of recovered 0.07 V-g-C_3N_4. These further demonstrate that the existence of Ce species facilitates the formation of V^{4+} and V^{3+} species. Moreover, XRD and FT-IR (electronic supplementary material, figures S3 and S4) measurements were conducted for the recovered $Ce_{0.07}$-0.07 V-g-C_3N_4 from the fourth run.

The structural properties of the recovered catalyst are nearly identical to those of fresh one, indicating the strong interactions between metal species and g-C_3N_4 support which accounts for high stability of $Ce_{0.07}$-0.07 V-g-C_3N_4 in the direct benzene hydroxylation. The excellent stability is because of abundant defects of g-C_3N_4 after cerium modification that improve the dispersion and stability of V species. Although the role of V^{3+} species remains to be further studied, the work gives an insight into the design of efficient catalysts for the titled reaction in future.

A possible reaction mechanism of benzene hydroxylation is proposed based on literature work [22]. Benzene is chemically absorbed onto the surface of g-C_3N_4, and then the surface dispersed V^{4+} species are oxidized by H_2O_2 to produce V^{5+}-O-O• radicals and H_2O. The main active V^{5+}-O-O• radicals are rapidly activated and react with absorbed benzene to gain the target phenol and V^{5+} is reduced to V^{4+}. At the same stage, the redox V^{5+}/V^{4+} is supported by Ce^{3+}/Ce^{4+} to accelerate the reaction into the next recycle.

4. Conclusion

In this work, we developed a facile method to synthesize cerium-doped V-g-C_3N_4 catalysts for the direct oxidation of benzene to phenol. The dispersion of vanadium species was distinctly improved after the addition of cerium species. Among the catalysts studied, $Ce_{0.07}$-0.07 V-g-C_3N_4 showed excellent catalytic performance with good reusability in the titled reaction, ascribed to the enhanced vanadium redox property, improved benzene adsorption ability and strong interactions between metal species and g-C_3N_4 support.

Data accessibility. The datasets supporting this article have been uploaded as part of the electronic supplementary material.

Authors' contributions. C.W., L.H. and M.W. performed the experiments and collected data. B.Y. and H.H. designed and directed the study and also wrote the manuscript. All authors gave final approval for publication.

Competing interests. The authors declare that they have no competing interests.

Funding. This work was supported by the National Natural Science Foundation of China (21371035, 21673046, 91645201 and 21473036).

Acknowledgement. We thank the Department of Chemistry, Fudan University, for providing the characterization facility for this study.

References

1. Chen JQ, Li J, Zhang Y, Gao SA. 2010 Transition metal substituted polyoxometalates and their application in the direct hydroxylation of benzene to phenol with hydrogen peroxide. *Res. Chem. Intermed.* **36**, 959–968. (doi:10.1007/s11164-010-0208-4)
2. Molinari R, Poerio T. 2010 Remarks on studies for direct production of phenol in conventional and membrane reactors. *Asia-Pac. J. Chem. Eng.* **5**, 191–206. (doi:10.1002/apj.369)
3. Leng Y, Ge HQ, Zhou CJ, Wang J. 2008 Direct hydroxylation of benzene with hydrogen peroxide over pyridine-heteropoly compounds. *Chem. Eng. J.* **145**, 335–339. (doi:10.1016/j.cej.2008.08.015)
4. Dong YL, Niu XY, Song WN, Wang D, Chen LQ, Yuan FL, Zhu YJ. 2016 Facile synthesis of vanadium oxide/reduced graphene oxide composite catalysts for enhanced hydroxylation of benzene to phenol. *Catalysts* **6**, 74–89. (doi:10.3390/catal6050074)
5. Zhang X, Li YX, Li GY, Hu CW. 2015 Preparation of Fe/activated carbon directly from rice husk pyrolytic carbon and its application in catalytic hydroxylation of phenol. *RSC Adv.* **5**, 4984–4992. (doi:10.1039/c4ra13248c)
6. Sobolev VI, Kharitonov AS, Paukshtis YA, Panov GI. 1993 Stoichiometric reaction of benzene with alpha-form of oxygen on FeZSM-5 zeolites mechanism of aromatics hydroxylation by N_2O. *J. Mol. Catal.* **84**, 117–124. (doi:10.1016/0304-5102(93)80090-H)
7. Tanarungsun G, Kiatkittipong W, Assabumrungrat S, Yamada H, Tagawa T, Praserthdam P. 2007 Fe(III), Cu(II), V(V)/TiO_2 for hydroxylation of benzene to phenol with hydrogen peroxide at room temperature. *J. Chem. Eng. Jpn.* **40**, 415–421. (doi:10.1252/jcej.40.415)
8. Xu J, Chen Y, Hong Y, Zheng H, Ma D, Xue B, Li Y-X. 2018 Direct catalytic hydroxylation of benzene to phenol catalyzed by vanadia supported on exfoliated graphitic carbon nitride. *Appl. Catal. A* **549**, 31–39. (doi:10.1016/j.apcata.2017.09.015)
9. Capocasa G, Olivo G, Barbieri A, Lanzalunga O, Di Stefano S. 2017 Direct hydroxylation of benzene and aromatics with H_2O_2 catalyzed by a self-assembled iron complex: evidence for a metal-based mechanism. *Catal. Sci. Technol.* **7**, 5677–5686. (doi:10.1039/c7cy01895a)
10. Tsuji T, Zaoputra AA, Hitomi Y, Mieda K, Ogura T, Shiota Y, Yoshizawa K, Sato H, Kodera M. 2017 Specific enhancement of catalytic activity by a dicopper core: selective hydroxylation of benzene to phenol with hydrogen peroxide. *Angew. Chem .Inter. Ed.* **56**, 7779–7782. (doi:10.1002/anie.201702291)
11. Han JW, Jung J, Lee YM, Nam W, Fukuzumi S. 2017 Photocatalytic oxidation of benzene to phenol using dioxygen as an oxygen source and water as an electron source in the presence of a cobalt catalyst. *Chem. Sci.* **8**, 7119–7125. (doi:10.1039/c7sc02495a)
12. Wang X, Meng B, Tan X, Zhang X, Zhuang S, Liu L. 2014 Direct hydroxylation of benzene to phenol using palladium-titanium silicalite zeolite bifunctional membrane reactors. *Ind. Eng. Chem. Res.* **53**, 5636–5645. (doi:10.1021/ie404163e)
13. Li Y, Li B, Geng L, Wang J, Wang Y, Huang J. 2015 The hydroxylation of aromatics with oxygen by vanadium catalysts supported on N-doped carbon materials. *Catal. Lett.* **145**, 1014–1021. (doi:10.1007/s10562-015-1478-7)
14. Borah P, Datta A, Kim Truc N, Zhao Y. 2016 $VOPO_4 \cdot 2H_2O$ encapsulated in graphene oxide as a heterogeneous catalyst for selective hydroxylation of benzene to phenol. *Green Chem.* **18**, 397–401. (doi:10.1039/c5gc01194a)
15. Wang H, Zhao M, Zhao Q, Yang Y, Wang C, Wang Y. 2017 In-situ immobilization of $H_5PMo_{10}V_2O_{40}$ on protonated graphitic carbon nitride under hydrothermal conditions: a highly efficient and reusable catalyst for hydroxylation of benzene. *Ind. Eng. Chem. Res.* **56**, 2711–2721. (doi:10.1021/acs.iecr.6b04371)
16. Peng G, Fu Z, Yin D, Zhong S, Yang Y, Yu N, Yin D. 2007 A promising coupled process of Pd/gamma-Al_2O_3-NH_4VO_3 catalyzing the hydroxylation of benzene with hydrogen peroxide produced in situ by an anthraquinone redox route. *Catal. Lett.* **118**, 270–274. (doi:10.1007/s10562-007-9183-9)

17. Jiang WF, Wang W, Wang HL, Li ZQ. 2009 Photooxidation of benzene to phenol by Al_2O_3-supported Fe(III)-5-sulfosalicylic acid (ssal) complex. *Catal. Lett.* **130**, 463–469. (doi:10.1007/s10562-009-9976-0)
18. Murata K, Yanyong R, Inaba M. 2005 Effects of vanadium supported on ZrO_2 and sulfolane on the synthesis of phenol by hydroxylation of benzene with oxygen and acetic acid on palladium catalyst. *Catal. Lett.* **102**, 143–147. (doi:10.1007/s10562-005-5846-6)
19. Jiang L, Yuan X, Pan Y, Liang J, Zeng G, Wu Z, Wang H. 2017 Doping of graphitic carbon nitride for photocatalysis: a review. *Appl. Catal. B-Environ.* **217**, 388–406. (doi:10.1016/j.apcatb.2017.06.003)
20. Han Q, Chen N, Zhang J, Qu L. 2017 Graphene/graphitic carbon nitride hybrids for catalysis. *Mater. Horizons* **4**, 832–850. (doi:10.1039/c7mh00379j)
21. Sun S, Liang S. 2017 Recent advances in functional mesoporous graphitic carbon nitride (mpg-C_3N_4) polymers. *Nanoscale* **9**, 10 544–10 578. (doi:10.1039/c7nr03656f)
22. Wang C, Hu L, Wang M, Ren Y, Yue B, He H. 2016 Vanadium supported on graphitic carbon nitride as a heterogeneous catalyst for the direct oxidation of benzene to phenol. *Chin. J. Catal.* **37**, 2003–2008. (doi:10.1016/s1872-2067(16)62496-8)
23. Jin RR, Hu SZ, Gui JZ, Liu D. 2015 A convenient method to prepare novel rare earth metal Ce-doped carbon nitride with enhanced photocatalytic activity under visible light. *Bull. Korean Chem. Soc.* **36**, 17–23. (doi:10.1002/bkcs.10001)
24. Paz DS, Damyanova S, Borges LR, Santos JBO, Bueno JMC. 2017 Identifying the adsorbed active intermediates on Pt surface and promotion of activity through the redox CeO_2 in preferential oxidation of CO in H_2. *Appl. Catal. A-Gen.* **548**, 164–178. (doi:10.1016/j.apcata.2017.08.012)
25. Lu S, Wang F, Chen C, Huang F, Li K. 2017 Catalytic oxidation of formaldehyde over CeO_2-Co_3O_4 catalysts. *J. Rare Earths* **35**, 867–874. (doi:10.1016/s1002-0721(17)60988-8)
26. Long ZY, Zhou Y, Chen GJ, Ge WL, Wang J. 2014 C_3N_4-$H_5PMo_{10}V_2O_{40}$: a dual-catalysis system for reductant-free aerobic oxidation of benzene to phenol. *Sci. Rep.* **4**, 3651. (doi:10.1038/srep03651)
27. Shijina AV, Renuka NK. 2009 Single step conversion of benzene to phenol using hydrogen peroxide over modified V_2O_5-Al_2O_3 systems. *React. Kinet. Catal. Lett.* **98**, 139–147. (doi:10.1007/s11144-009-0079-0)
28. Xu J, Jiang Q, Chen T, Wu F, Li YX. 2015 Vanadia supported on mesoporous carbon nitride as a highly efficient catalyst for hydroxylation of benzene to phenol. *Catal. Sci. Technol.* **5**, 1504–1513. (doi:10.1039/c4cy01373e)
29. Yang H, Jin Z, Hu H, Bi Y, Lu G. 2018 Ni-Mo-S nanoparticles modified graphitic C_3N_4 for efficient hydrogen evolution. *Appl. Surf. Sci.* **427**, 587–597. (doi:10.1016/j.apsusc.2017.09.021)
30. Ma JQ, Yang QF, Wen YZ, Liu WP. 2017 Fe-g-C_3N_4/graphitized mesoporous carbon composite as an effective Fenton-like catalyst in a wide pH range. *Appl. Catal. B-Environ.* **201**, 232–240. (doi:10.1016/j.apcatb.2016.08.048)
31. Zhu TT *et al.* 2015 Synthesis of g-C_3N_4/Ag_3VO_4 composites with enhanced photocatalytic activity under visible light irradiation. *Chem. Eng. J.* **271**, 96–105. (doi:10.1016/j.cej.2015.02.018)
32. Xu J, Jiang Q, Shang JK, Wang Y, Li YX. 2015 A Schiff-base-type vanadyl complex grafted on mesoporous carbon nitride: a new efficient catalyst for hydroxylation of benzene to phenol. *RSC Adv.* **5**, 92 531–92 538. (doi:10.1039/c5ra21438f)
33. Liu Y, Jiaa C, Do H. 1999 Correlation of deposition and IR properties of amorphous carbon nitride films. *Surf. Coat. Technol.* **115**, 95–102. (doi:10.1016/s0257-8972(99)00044-4)
34. Xia BY, Yan Y, Li N, Wu HB, Lou XW, Wang X. 2016 A metal-organic framework-derived bifunctional oxygen electrocatalyst. *Nat. Energy* **1**, 15 006–15 050. (doi:10.1038/nenergy.2015.6)
35. Furukawa H, Cordova KE, O'Keeffe M, Yaghi OM. 2013 The chemistry and applications of metal-organic frameworks. *Science* **341**, 974–983. (doi:10.1126/science.1230444)
36. Hu SZ, Ma L, You JG, Li FY, Fan ZP, Lu G, Liu D, Gui JZ. 2014 Enhanced visible light photocatalytic performance of g-C_3N_4 photocatalysts co-doped with iron and phosphorus. *Appl. Surf. Sci.* **311**, 164–171. (doi:10.1016/j.apsusc.2014.05.036)
37. Yang DX, Jiang T, Wu TB, Zhang P, Han HL, Han BX. 2016 Highly selective oxidation of cyclohexene to 2-cyclohexene-1-one in water using molecular oxygen over Fe-Co-g-C_3N_4. *Catal. Sci. Technol.* **6**, 193–200. (doi:10.1039/c5cy01177a)
38. Diodati S, Negro E, Vezzu K, Di Noto V, Gross S. 2016 Oxygen reduction reaction and X-ray photoelectron spectroscopy characterisation of carbon nitride-supported bimetallic electrocatalysts. *Electrochim. Acta* **215**, 398–409. (doi:10.1016/j.electacta.2016.08.060)
39. Zhao LK, Li CT, Wang Y, Wu HY, Gao L, Zhang J, Zeng GM. 2016 Simultaneous removal of elemental mercury and NO from simulated flue gas using a CeO_2 modified V_2O_5-WO_3/TiO_2 catalyst. *Catal. Sci. Technol.* **6**, 6076–6086. (doi:10.1039/c5cy01576f)
40. Martinez-Huerta MV, Coronado JM, Fernandez-Garcia M, Iglesias-Juez A, Deo G, Fierro JLG, Banares MA. 2004 Nature of the vanadia-ceria interface in V^{5+}/CeO_2 catalysts and its relevance for the solid-state reaction toward $CeVO_4$ and catalytic properties. *J. Catal.* **225**, 240–248. (doi:10.1016/j.jcat.2004.04.005)
41. Zhang SC, Ruan YF, Jia GZ, Feng ZH, Liu ZP, Pei LB. 2014 Blue-emitting properties of Ce^{3+} doped YVO_4 under ultraviolet excitation. *J. Inorg. Mater.* **29**, 1067–1072. (doi:10.15541/jim20140060)
42. Lee CH, Lin TS, Mou CY. 2003 VO^{2+} ions immobilized on functionalized surface of mesoporous silica and their activity toward the hydroxylation of benzene. *J. Phys. Chem. B* **107**, 2543–2551. (doi:10.1021/j6703f)p02)
43. Beche E, Charvin P, Perarnau D, Abanades S, Flamant G. 2008 Ce 3d XPS investigation of cerium oxides and mixed cerium oxide ($Ce_xTi_yO_z$). *Surf. Interface Anal.* **40**, 264–267. (doi:10.1002/sia.2686)
44. Chen X, Zhao WG, Wang F, Xu J. 2012 Preparation and characterization of vanadium(IV) oxide supported on SBA-15 and its catalytic performance in benzene hydroxylation to phenol using molecular oxygen. *J. Nat. Gas Chem.* **21**, 481–487. (doi:10.1016/s1003-9953(11)60394-0)
45. Tanarungsun G, Yamada H, Tagawa T, Kiatkittipong W, Praserthdam P, Assabumrungrat S. 2011 Partial oxidation of benzene catalyzed by vanadium chloride in novel reaction–extraction–regeneration system. *Chem. Eng. Process.* **50**, 53–58. (doi:10.1016/j.cep.2010.11.006)
46. Boehm HP. 1994 Some aspects of the surface chemistry of carbon blacks and other carbons. *Carbon* **32**, 759–769. (doi:10.1016/0008-6223(94)90031-0)
47. Lahaye J. 1998 The chemistry of carbon surfaces. *Fuel* **77**, 543–547. (doi:10.1016/s0016-2361(97)00099-9)